SINTEF
PROCEEDINGS 6

14th International Conference on CFD in
Oil & Gas, Metallurgical and Process Industries
SINTEF, Trondheim, Norway, October 12–14, 2020

Proceedings from the 14th International Conference on CFD in Oil & Gas, Metallurgical and Process Industries

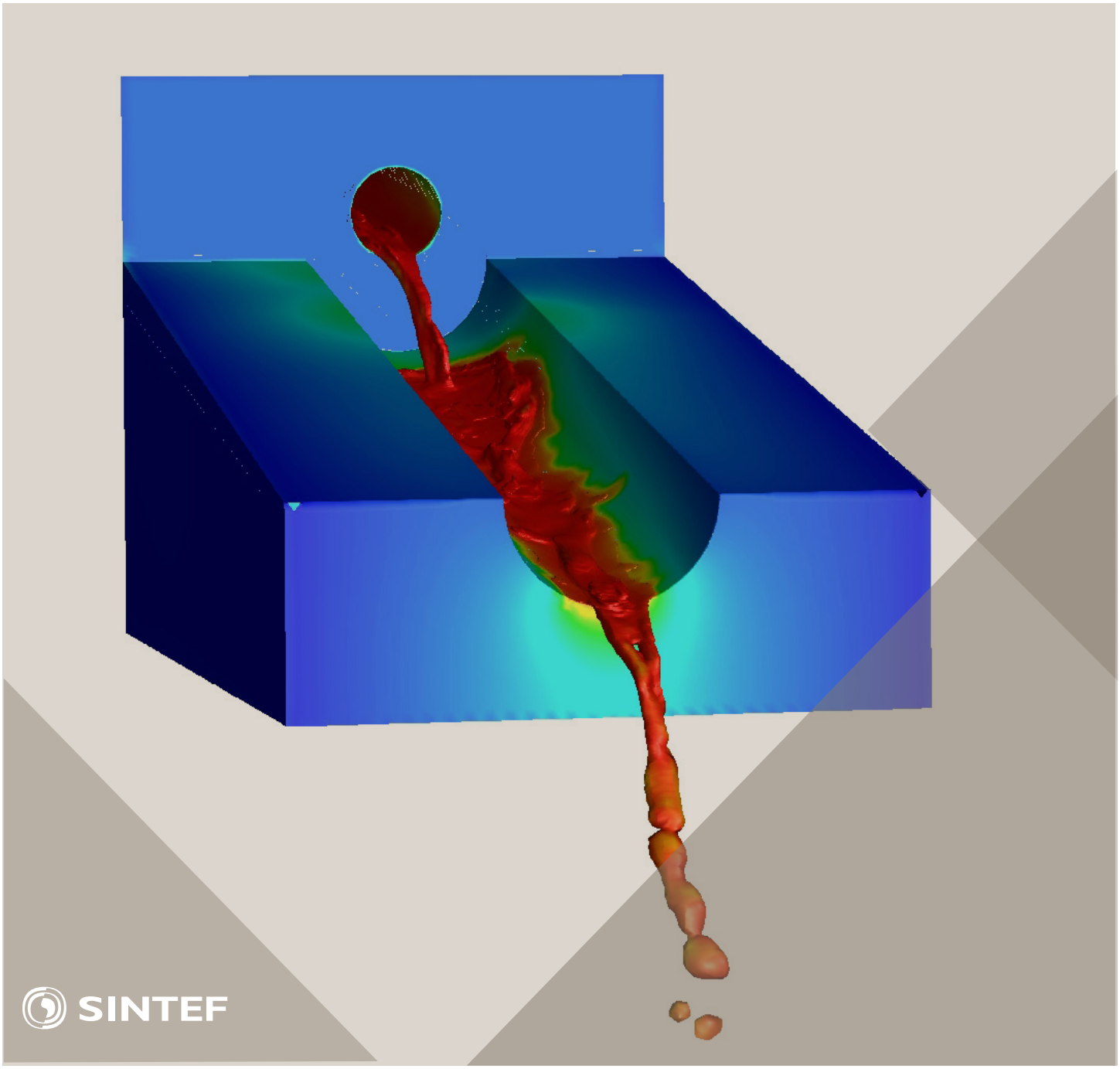

SINTEF Proceedings

Editors:
Jan Erik Olsen, Jan Hendrik Cloete and Stein Tore Johansen

Proceedings from the 14th International Conference on CFD in Oil & Gas, Metallurgical and Process Industries

SINTEF, Trondheim, Norway
October 12–14, 2020

SINTEF Academic Press

SINTEF Proceedings 6
Editors: Jan Erik Olsen, Jan Hendrik Cloete and Stein Tore Johansen

Proceedings from the 14th International Conference on CFD in Oil & Gas, Metallurgical and Process Industries, SINTEF, Trondheim, Norway, October 12–14, 2020

Keywords:
CFD, fluid dynamics, modelling

Cover illustration: Tapping of metal by Jan Erik Olsen

ISSN 2387-4295 (online)
ISBN 978-82-536-1684-1 (pdf)

SINTEF Academic Press
Address: Børrestuveien 3
PO Box 124 Blindern
N-0314 OSLO
Tel: +47 40 00 51 00

www.sintef.no/community
www.sintefbok.no

IMPROVEMENT OF EULER-EULER SIMULATION OF TWO-PHASE FLOW BY PARTICLE-CENTER-AVERAGED METHOD

Hongmei Lyu[1, 2]* , Fabian Schlegel, Roland Rzehak, Dirk Lucas

[1]Helmholtz-Zentrum Dresden - Rossendorf, Institute of Fluid Dynamics, Bautzner Landstrasse 400, D-01328 Dresden, Germany

[2]Technische Universität Dresden, Faculty of Mechanical Engineering, Institute of Power Engineering, D-01062 Dresden, Germany

* E-mail: h.lyu@hzdr.de

ABSTRACT

The standard Euler-Euler modelling is based on the phase-averaged method and the forces of the bubble are the function of gas volume fraction. However, the closure models for the forces are developed based on the measured bubble trajectory and the assumption that the forces act on bubble center. This inconsistency can lead to a nonphysical gas concentration in the center or in the near wall region of a pipe if the bubble diameter is larger than the mesh size. In addition, mesh independent solutions may not exist in these cases.

In the present contribution, particle-center-averaged method is used in the average of the parameters for the disperse phase and the forces for bubble is changed to act on the bubble center. In this approach, the number density of the bubble centers is one of the solution variables. The gas volume fraction can be calculated from the number density by a diffusion-based method, which is much easier to implement in the CFD codes using the unstructured grids like OpenFOAM. A physically motivated model for the wall-contact force is introduced to ensure that the bubble centers cannot come arbitrarily close to walls.

The remedy of the issues with the conventional phase-averaged two-fluid model is demonstrated using a simplified two-dimensional test case. Furthermore, a comparison is made for pipe flow cases where experimental data are available. The results show that the particle-center-averaged method can help to decrease the over-prediction of the peaks in the gas volume fraction profiles and obtain the mesh independent solutions in the Euler-Euler modelling.

Keywords: Particle-center-average, number density, bubble dimension, diffusion equation, deformation force model, equation of motion.

NOMENCLATURE

Greek Symbols

α	Volume fraction, [-].
β	Bubble volume fraction attaching all bubble volume to its center, [-].
ρ	Mass density, [$kg \cdot m^{-3}$].
τ	Diffusion time, [s].
σ	Surface tension coefficient, [$N \cdot m^{-1}$].

Latin Symbols

d	Bubble diameter, [m].
$\boldsymbol{f}$	Interfacial forces, [$N \cdot m^{-3}$].
$\boldsymbol{g}$	Acceleration of gravity, [$m \cdot s^{-2}$].
J	Superficial velocity, [$m \cdot s^{-1}$].
n	Number density of bubble centers, [m^{-3}].
N	The number of bubbles in the system, [-].
p	Pressure, [Pa].
r	Bubble radial, [m].
$\mathbf{S}$	Viscous stress tensor, [$N \cdot m^{-2}$].
$\mathbf{T}$	Reynold stress tensor, [$N \cdot m^{-2}$].
t	Time, [s].
$\boldsymbol{u}$	Velocity, [$m \cdot s^{-1}$].
V	Bubble volume, [m^3].
X	Phase indicator function, [-].

Sub/superscripts

air	Air.
B	Bubble.
c	Continuous phase.
d	Disperse phase.
diff	diffusion
deformation	Deformation force.
i	Index *i.*
interfacial	Interfacial force.
lift	Lift force.
water	Water.

INTRODUCTION

Two-phase flows are widely encountered in chemical engineering, energy production and conversion, oil and gas industries and biotechnology (Lucas et al., 2010). However, many flow mechanisms are still unclear due to their high complexity. Experimental investigations on the two-phase flows are challenging, costly and time-consuming due to the need to discriminate the two phases. In comparison, simulations provide a more accessible way to study these flows, but they invariably rely on models. Among the simulation methods, the Eulerian two-fluid model shows the advantages for the simulation of the bubbly flows up to the industrial dimensions.

In the standard Eulerian framework, the fluids are treated as the interpenetrating continua using a phase indicator function to identify each phase. In this way, the forces acting on the bubble are distributed to the entire region covered by it. As a consequence, the coherent motion of the bubble as a whole is not enforced. As a result, some unphysical phenomena appear in the simulation results of the standard Euler-Euler modelling. For example, an over-prediction of the peak of the gas volume fraction can appear in the pipe center if the bubble diameter is

larger than the mesh size (Tomiyama et al., 2003). A similar phenomenon can occur in the near wall region such that the peak of gas volume fraction locates directly on the wall (Rzehak et al., 2017).

A feasible way to recover the inconsistencies in the two-fluid model is by using the particle-center-averaged method to average the parameters of disperse phase. This approach has been applied to introduce bubble geometry in the simulation of the wall-bounded bubbly flow (Moraga et al., 2006). In this method, the delta function indicating the location of the bubble center is involved explicitly (Biesheuvel et al., 1989, Biesheuvel et al., 1990, Sangani et al., 1993, Moraga et al., 2006) or implicitly (Zhang et al., 1994a, Prosperetti, 1998) in the averaging. As a result, the mass and momentum of each bubble are assigned to its center. Also the forces act in the bubble center. In addition, the number density of the bubble centers is the primary variable and the gas volume fraction is derived from it.

The calculation of the gas volume fraction is a key issue in the two-fluid modelling based on the particle-center-averages. The coarse graining methods in the CFD-DEM modelling (Khawaja et al., 2012, Peng et al., 2014) and the interphase coupling methods of the Euler-Lagrange modelling (Kitagawa et al., 2001, Hu et al., 2008) can be borrowed to deal with this issue. Among these methods, the "small particle approximation" used in Zhang and Prosperetti's research (Zhang et al., 1994a, Prosperetti, 1998) assigns all the volume of the disperse element to the mesh cell containing its center. This is not appropriate for the case of interest in the present study where the bubble size exceeds the spacing of the numerical mesh. Analytical approaches, which compute the volume of the overlapped region between the bubble and the Euler mesh are easy to implement for the structured meshes but difficult to use on the unstructured ones. Moreover, the analytical method can cause large fluctuations in the distribution of the gas volume fraction when the mesh spacing is smaller than the bubble diameter (Sun et al., 2015b). The convolution method (Kitagawa et al., 2001, Xiao et al., 2011) and the diffusion-based method (Sun et al., 2015b, Sun et al., 2015a) are two promising approaches for the calculation of the gas volume fraction. In the convolution method, the gas volume fraction is calculated as a weighted average by using a kernel function as the weight factor. However, it is complicated to deal with the kernel function near the curved boundaries or in corners of the domain where boundaries meet non-orthogonally and to implement it in a code for the unstructured meshes and parallel computation (Sun et al., 2015b). In the diffusion-based method, the gas volume fraction is the solution of a diffusion equation. This method is easy to implement for the cases using the structured or unstructured meshes and serial or parallel processing. In addition, it gives similar results as the convolution method with a Gaussian kernel function by selecting a suitable diffusion time (Sun et al., 2015b). Hence, it is used for the calculation of the gas volume fraction in this study.

When the particle-center-averaged method is used, the averaged momentum equation obtained for the disperse phase is slightly different. In the standard Euler-Euler modelling, this equation is derived by averaging the local instantaneous momentum equation of the disperse phase. In contrast, Zhang and Prosperetti et al. (Zhang et al., 1994a, Zhang et al., 1994b, Prosperetti, 1998) derived this equation by averaging the particle equation of motion directly. The disperse phase momentum equations derived by these two methods have slightly different meanings. In the standard Euler-Euler modelling, the equation shows the momentum balance of the disperse phase material entirely contained inside the control volume. The equation derived by Zhang and Prosperetti et al. instead displays the momentum balance of the disperse phase material, which belongs to the particles with their centers located inside the control volume. For the gas-liquid bubbly flow, since the mass and viscosity of the disperse bubbles are small, the latter method is recommended (Zhang et al., 1994a, Zhang et al., 1994b, Zhang et al., 1995) to avoid involving the constitutive equations of the gas material. Therefore, the momentum equation derived by the latter method is used for gas phase in present study.

In this work, the particle-center-averaging is applied to the dispersed phase and the phase-averaging is used for the continuous phase. The idea of using the different averaging approaches for the various phases was introduced in the study of two-phase flow before (Zhang et al., 1994a, Prosperetti, 1998, Moraga et al., 2006). The momentum equation for the disperse phase derived from the equation of motion of the bubbles shows explicitly that the bubbles respond to pressure and stress of the continuous phase. Furthermore, the models for interfacial forces are changed to be functions of the number density of the bubble centers. In addition, to avoid the bubble centers to come arbitrarily close to walls, a wall-contact force is introduced. The deformation force model of Lucas et al. (Lucas et al., 2007) is adapted for oblate ellipsoidal bubbles and used in the simulation.

In present study, the particle-center-averaged method and the deformation force model are implemented in OpenFOAM-6. In order to evaluate the Euler-Euler modelling based on the particle-center-averages, a simple two-dimensional test case is used first and then comparisons between predictions and experimental measurements are made. The novelty of this research lies in combining the particle-center-averaged method with the Helmholtz-Zentrum Dresden-Rossendorf baseline closure model (Rzehak et al., 2017) for the Euler-Euler modelling and determining the gas volume fraction based on a diffusion equation.

TWO-FLUID MODEL FRAMEWORK BASED ON PARTICLE-CENTER-AVERAGED METHOD

This section introduces the theory of the applied Euler-Euler model. As mentioned before, the phase-average and the particle-center-average are used to average the continuous and the disperse phases respectively. The difference between this method and the standard Euler-Euler method employing the phase-average for both phases will be explained in detail. Both phases are taken as incompressible and a fixed monodisperse bubble size is assumed.

Continuity equations

Since the continuous phase uses the phase-average method, its continuity equation remains the same as in the standard Euler-Euler modelling (Drew et al., 1998, Prosperetti, 1998)

$$\frac{\partial \alpha_c}{\partial t} + \nabla \cdot \alpha_c \overline{\boldsymbol{u}_c}^x = 0. \quad (1)$$

In this equation, the volume fraction is defined as

$$\alpha_c = \int_{C^N} X_c P^N dC^N \ , \quad (2)$$

while the ensemble phase-averaged velocity of the continuous phase $\overline{\boldsymbol{u}_c}^x$ is given by

$$\overline{\boldsymbol{u}_c}^x = \frac{\int_{C^N} \boldsymbol{u}_c X_c P^N dC^N}{\alpha_c} \ . \quad (3)$$

In these equations, X_c is the phase-indicator function for the continuous phase. P^N is the probability density function of the set of all possible states of N bubbles, C^N. Here and the following, the notation with an overbar and nearby x is used to indicate ensemble phase-averaged variables.

Employing particle-center-averages, the continuity equation for the disperse phase is a transport equation for the number density of the bubble centers (Prosperetti, 1998)

$$\frac{\partial n}{\partial t} + \nabla \cdot (n \langle \boldsymbol{u}_d \rangle) = 0. \quad (4)$$

The definition of this number density is

$$n(\boldsymbol{x}, t) = \int P(\boldsymbol{x}, \boldsymbol{u}_d, t)\, d\boldsymbol{u}_d \ , \quad (5)$$

where $P(\boldsymbol{x}, \boldsymbol{u}_d, t)$ is the probability of finding a bubble centered at $\boldsymbol{x}$ with center-of-mass velocity $\boldsymbol{u}_d$ at time t. It is related to P^N as the integral over all bubbles except one. From the definition, we can see that the number density is non-zero only for those control volumes that may contain a bubble center.

In Eq. (4), $\langle \boldsymbol{u}_d \rangle$ is the particle-center-averaged velocity of the bubbles. It is defined as

$$\langle \boldsymbol{u}_d \rangle (\boldsymbol{x}, t) = \frac{\int P(\boldsymbol{x}, \boldsymbol{u}_d, t) \boldsymbol{u}_d \, d\boldsymbol{u}_d}{n(\boldsymbol{x}, t)} . \quad (6)$$

By using Eq. (4) as the continuity equation, information on the bubble centres will be accessible.

Momentum equations

For incompressible Newtonian flow, the momentum equation for the continuous phase is (Prosperetti, 1998)

$$\begin{aligned} \frac{\partial \alpha_c \rho_c \overline{\boldsymbol{u}_c}^x}{\partial t} + \nabla \cdot (\alpha_c \rho_c \overline{\boldsymbol{u}_c}^x \overline{\boldsymbol{u}_c}^x) \\ = -\alpha_c \nabla \overline{p_c}^x + \alpha_c \nabla \cdot \overline{\boldsymbol{S}_c}^x \\ + \nabla \cdot \alpha_c \overline{\boldsymbol{T}_c}^x + \overline{\boldsymbol{f}_c^{\text{interfacial}}}^x \\ + \alpha_c \rho_c \boldsymbol{g} \ . \end{aligned} \quad (7)$$

The momentum equation for the disperse phase is (Prosperetti, 1998)

$$\begin{aligned} \frac{\partial (\beta_d \rho_d \langle \boldsymbol{u}_d \rangle)}{\partial t} + \nabla \cdot (\beta_d \rho_d \langle \boldsymbol{u}_d \rangle \langle \boldsymbol{u}_d \rangle) \\ = -\beta_d \nabla \overline{p_c}^x + \beta_d \nabla \cdot \overline{\boldsymbol{S}_c}^x \\ + \nabla \cdot (\beta_d \langle \boldsymbol{T}_d \rangle) + \beta_d \rho_d \boldsymbol{g} \\ + \langle \boldsymbol{f}_d^{\text{interfacial}} \rangle \ , \end{aligned} \quad (8)$$

where

$$\beta_d \ = n V_d \ . \quad (9)$$

It is important to note that β_d is not the disperse phase volume fraction. The latter is related to the bubble number density by a convolution

$$\alpha_d(\boldsymbol{x}) \ = \iiint n(\boldsymbol{x_0}) X_d(\boldsymbol{x_0}) d\boldsymbol{x_0} \ , \quad (10)$$

where $X_d(\boldsymbol{x_0})$ is the phase indicator function in the location of $\boldsymbol{x} = \boldsymbol{x_0}$.

The difference between above momentum equations and those in the standard Euler-Euler modelling lies in the following aspects.

1) In the viscous stress term, the parameters related to the volume fraction (α_c and β_d) are outside of the divergence operator.

2) The momentum equation of the disperse phase explicitly shows the response of the bubbles to the pressure and viscous stress of the continuous phase, since the equation is derived from the bubble equation of motion. In this condition, no additional closure model for the pressure or stress of gas phase is required.

3) The momentum equation of the disperse phase is related to the bubble number density instead of the gas volume fraction.

Models for Interfacial forces and turbulence

The relation of the interfacial forces in Eqs. (7) and (8) is

$$\overline{\boldsymbol{f}_c^{\text{interfacial}}}^x \ = -\langle \boldsymbol{f}_d^{\text{interfacial}} \rangle \ . \quad (11)$$

The selected correlations for the interfacial forces according to the HZDR baseline model (Rzehak et al., 2017) are listed in Table 1. In the simulations using the standard Euler-Euler modelling in OpenFOAM-6, it was found necessary to apply a damping for the lift force within the distance of one bubble diameter from the wall (see Fig. 1 below). For comparability, this wall-damped lift force is used for the particle-center-averaged simulations as well throughout this study except where specifically noted elsewise. No such damping was mentioned in previous simulations with the HZDR baseline model using ANSYS CFX.

Table 1: Selected models for interfacial forces in simulation

Interfacial force	Selected model
Drag force	Ishii et al. (1979)
(Shear-) lift force	Tomiyama et al. (2002) with cosine wall damping
Turbulent dispersion force	Burns et al. (2004)
Wall (-lift) force	Hosokawa et al. (2002)
Virtual mass force	Constant coefficient, $C_{vm} = 0.5$

The interfacial force models in the Euler-Euler simulations based on the particle-center-averaged method should be expressed as functions of the number density of the bubble centers rather the gas volume

fraction. This conversion is achieved by the following formulation

$$f(n) = \frac{nV_d}{\alpha} f(\alpha), \tag{12}$$

where $f(n)$ and $f(\alpha)$ are the interfacial forces as functions of the number density of the bubble centers and the gas volume fraction, respectively.

Furthermore, an additional wall-contact force must be introduced to avoid the bubble centers coming unphysically close to the wall. The deformation force model proposed by Lucas et al. (Lucas et al., 2007) is changed to be applicable for the bubbles with a more general oblate ellipsoidal shape and used in the simulation. The model reads

$$\begin{aligned} &f_{\text{deformation}} \\ &= -2\pi r_B \sigma n \left[-\frac{1}{x^2} \right. \\ &+ \frac{1}{1-x^3} \left(2x\sqrt{1-x^3}\,\operatorname{arctanh}\sqrt{1-x^3} \right. \\ &\left. \left. - \frac{3}{2}x + \frac{3}{2}x^4 \frac{\operatorname{arctanh}\sqrt{1-x^3}}{\sqrt{1-x^3}} \right) \right]. \end{aligned} \tag{13}$$

Both laminar and turbulent flows of the continuous phase are considered. In the turbulent case, the turbulent dispersion force and the *k-ω* SST turbulent model are employed together with the bubble-induced turbulence model of Ma et al. (Ma et al., 2017). The flow of the disperse phase is assumed to be laminar because the gas viscosity and density are much smaller than those of the liquid.

Diffusion-based method for gas volume fraction calculation

In this study, a diffusion-based method (Sun et al., 2015b, Sun et al., 2015a) is used to compute the gas volume fraction from the number density of the bubble centers. In this method, the gas volume fraction is calculated by solving a diffusion equation

$$\frac{\partial \alpha_d}{\partial \tau} - \nabla \cdot \left(C_{diff} \nabla \alpha_d \right) = 0 \tag{14}$$

with an initial condition

$$\alpha_d(x, \tau = 0) = n(x, \tau = 0) V_d \,. \tag{15}$$

The diffusion coefficient C_{diff} is set to $1 m^2 \cdot s^{-1}$ in this study. The variable τ is a pseudo-time, independent of physical time and the diffusion time $\tau = T$ up to which Eq. (13) is integrated determines the size of the diffusion domain.

The appropriate size of the diffusion domain remains an open question. Previously, it has been set to be 3 to 6 times the diameters of disperse element (Deen et al., 2004, Sun et al., 2015b, Sun et al., 2015a). This size can exceed the bubble size since the paths of the bubble motions may exhibit oscillations. In this study, an optimal diffusion time is determined by comparing the theoretical distribution of the gas volume fraction for a stream of spherical bubbles and the distribution of the gas volume fraction calculated by the diffusion equation.

The theoretical gas volume fraction distribution for a stream of spherical bubbles is (Lubchenko et al., 2018)

$$\alpha_d(x) = \alpha_{max} - \frac{\alpha_{max}}{r_B^2} (x - x_0)^2 \tag{16}$$

where the peak of the gas volume fraction, α_{max}, is related to the frequency of bubble injection.

The one-dimensional solution of Eq. (14) is (Haberman, 2012)

$$\begin{aligned} &\alpha_d(x, \tau) \\ &= \int_{-\infty}^{+\infty} nV_d \delta(x - x_0) \\ &\times \frac{1}{\sqrt{4\pi\tau}} \exp\left[-\frac{(x - x_0)^2}{4\tau} \right] dx_0 \,, \end{aligned} \tag{17}$$

which is seen to be the convolution of the initial δ –gas volume distribution with a Gaussian kernel.

An optimal diffusion time is determined by minimizing the root-mean-square deviation between $\alpha_d(x)$ and $\alpha_d(x, \tau)$ given by Eqs. (16) and (17), respectively. The Matlab optimization function *fminbnd( )* is used for this purpose. The resulting optimized diffusion time is

$$T = \frac{d_B^2}{30 C_{diff}} \,. \tag{18}$$

The gas volume fraction calculated using this optimized time is expected to have the most similar shape as the theoretical distribution (Eq. (16)).

ILLUSTRATION OF THE EULER-EULER MODELLING METHOD BASED ON THE PARTICLE-CENTER-AVERAGES

In this section, the advantages of the Euler-Euler simulation based on the particle-center-averaged method over the standard Euler-Euler modelling are illustrated by a simplified test case. Gas and liquid are taken to be air and water from here on and the indices denoting the phases are adapted accordingly.

Geometry and simulation set up

A two-dimensional test case similar to that used in Tomiyama et al (2003) is employed. The domain is a rectangle with a size of 0.03 m×0.5 m (see Fig. **1** a)).

A stream of bubbles is injected from the center of the shorter side. The gas volume fraction at inlet for the cases simulated by the standard Euler-Euler modelling can be seen in Fig. **1** b)). The lateral length covered by the gas volume fraction at the inlet shows the dimension of one bubble. The inlet liquid velocity is a parabolic profile (see Fig. **1** c)) to introduce a shear flow field. The inlet gas velocity is uniform with a value of $0.18\ m \cdot s^{-1}$.

For Euler-Euler simulations based on the particle-center-averages, the inlet number density of the bubble centers is non-zero only in the center mesh. Its value is calculated to obtain the same inlet gas flow rate as the cases simulated by the standard Euler-Euler modelling. For a uniform mesh and uniform inlet gas velocity, it is given by

$$n = \frac{1}{V_d}\sum_{i=1}^{M} \alpha_{air,i} \ , \qquad (19)$$

where M is the number of mesh cells at the inlet and V_d is the volume of the bubble.

Mesh sensitivity analysis

To reveal the numerical problems caused by the inconsistencies in the standard Euler-Euler modelling, the mesh sensitivity is analyzed in the simulation using the standard Euler-Euler modelling and the Euler-Euler simulation based on the particle-center-averaged method.

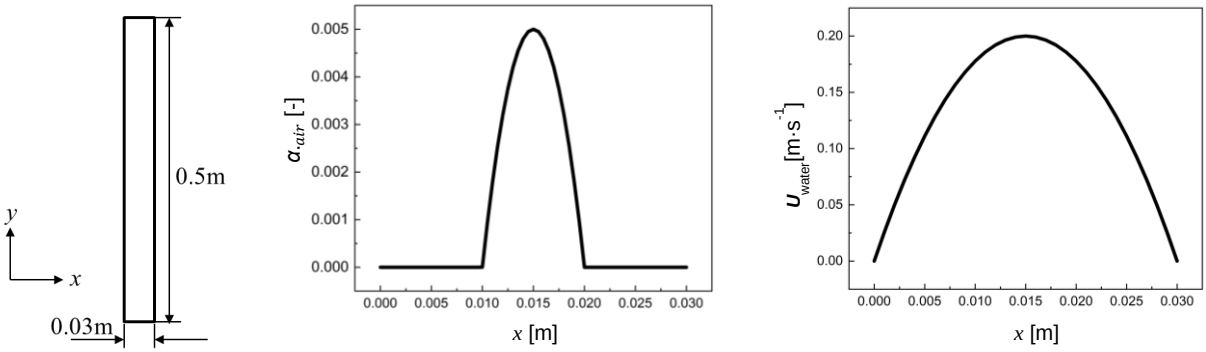

a) Geometry b) Inlet gas volume distribution c) Inlet liquid velocity distribution

Figure 1: Geometry and inlet settings

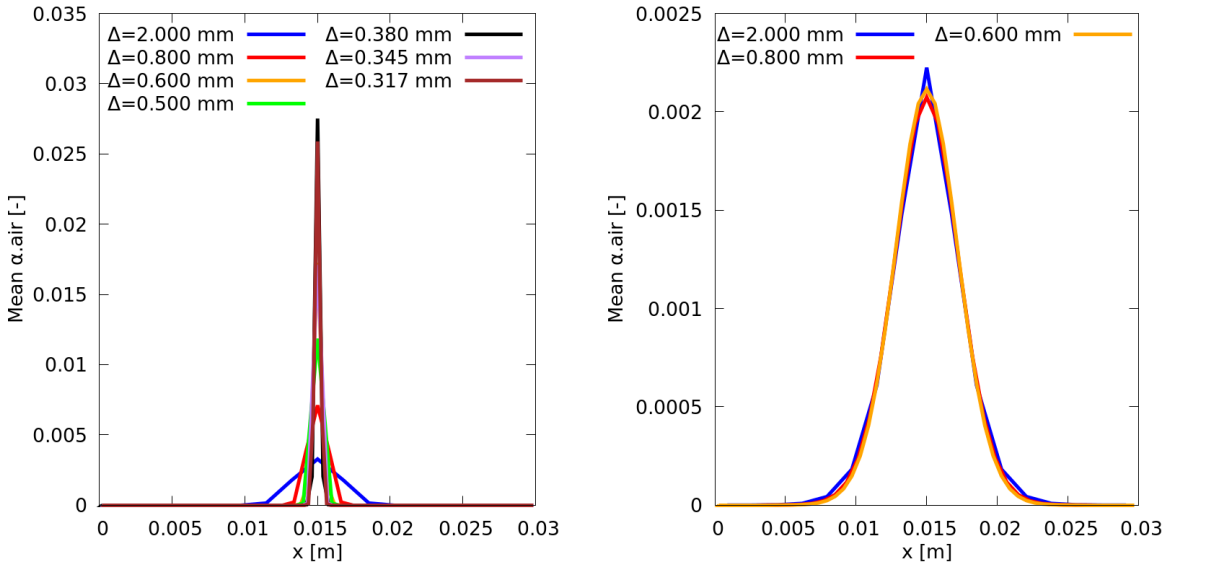

a) Standard Euler-Euler modelling b) Euler-Euler modelling based on particle-center-averages

Figure 2: Mesh sensitivity analysis in laminar flow case at a height y = 0.4 m (Δ : mesh size)

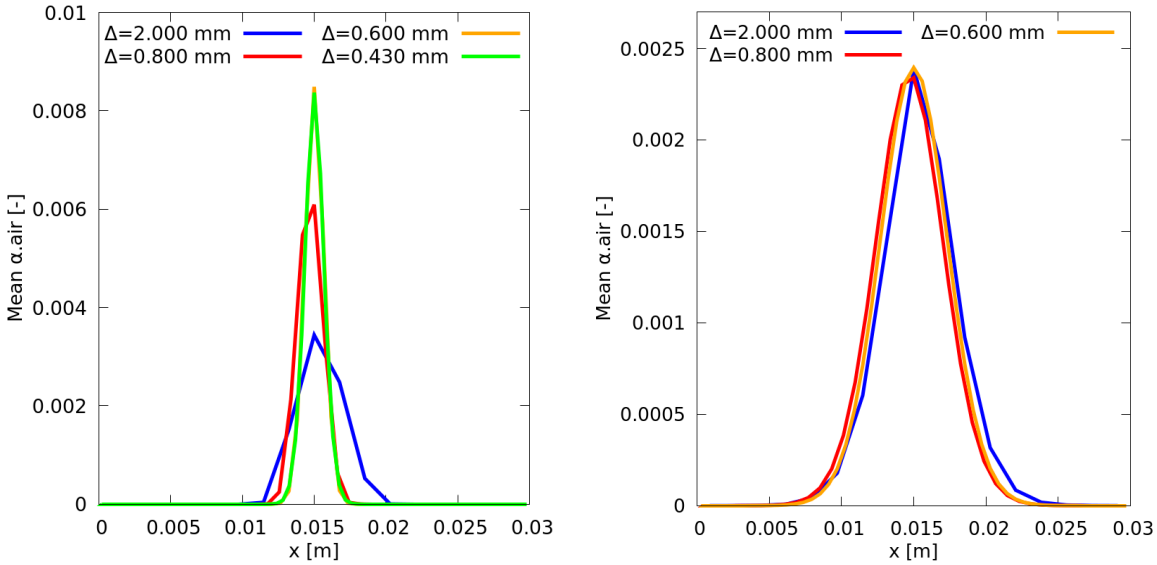

a) Standard Euler-Euler modelling b) Euler-Euler modelling based on particle-center-average

Figure 3: Mesh sensitivity analysis in turbulent flow case at a height y = 0.4 m (Δ : mesh size)

In this analysis, the bubble diameter is taken as 10 mm, while the coarsest spacing of the numerical grids $\Delta = 2$ mm. The simulation results at a height y = 0.4 m above the inlet are shown.

Laminar flow

The mesh sensitivity analysis of laminar simulation results can be seen in Fig. 2. In the results for the standard Euler-Euler modelling, the peak of the gas volume fraction increases continuously with decreasing mesh size (see Fig. 2 a)). Therefore, the mesh independent results are not found. This reason for the phenomenon is that the lift force is distributed to the cells of the numerical mesh covered by the bubble, which drives the gas in the mesh cells located at the bubble edge towards the bubble center, even though the bubble center does not move in the lateral direction. This phenomenon becomes more significant when the mesh is refined.

In comparison, in the results of the Euler-Euler simulation based on the particle-center-averaged method, the peak of the gas volume fraction does not increase upon refining the mesh (see Fig. 2 b)) since the lift force acts on the bubble center. As a result, the solution obtained with a mesh size of 0.8mm can be regarded as mesh independent solution. This means that in the laminar flow condition, the particle-center-averaged method remedies the numerical deficiency of the standard Euler-Euler approach and provides a mesh independent solution.

Turbulent flow

Upon including the turbulent dispersion force, the mesh independent solutions exist in both cases (see Fig. 3) since this force smoothes the nonphysical peak of gas volume fraction in the standard Euler-Euler modelling. The solutions for meshes with 0.6 mm and 0.8 mm can be regarded as mesh independent for the standard Euler-Euler modelling and the particle-center-average based Euler-Euler simulations, respectively. However, the nonphysical behaviours are still visible in the results of the standard Euler-Euler modelling.

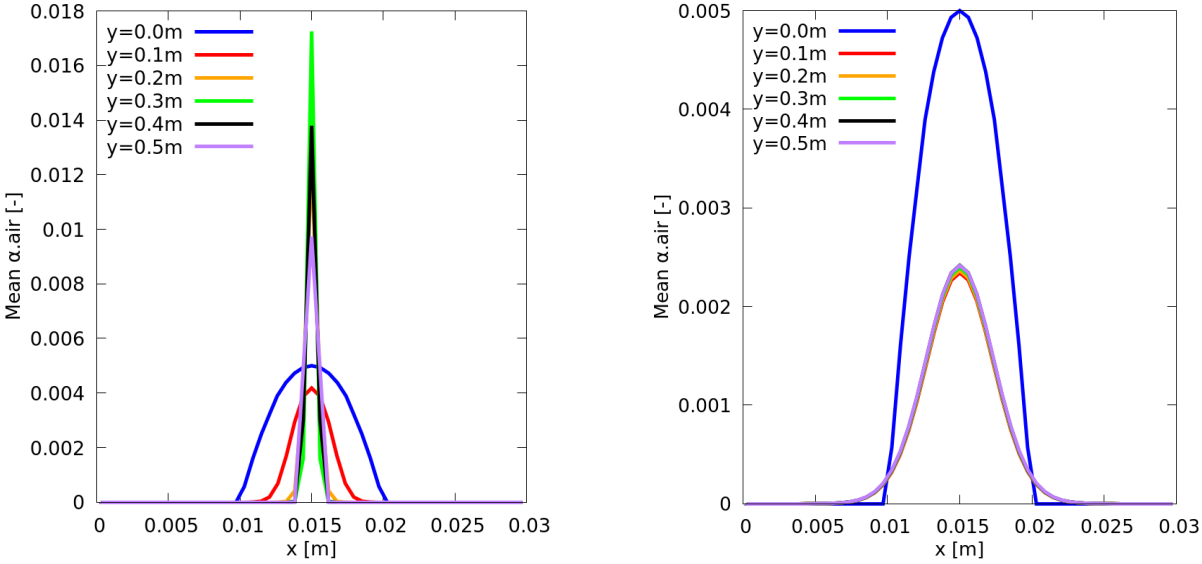

a) Standard Euler-Euler modelling b) Euler-Euler simulation based on particle-center-average

Figure 4: Lateral gas volume fraction distribution in laminar flow case

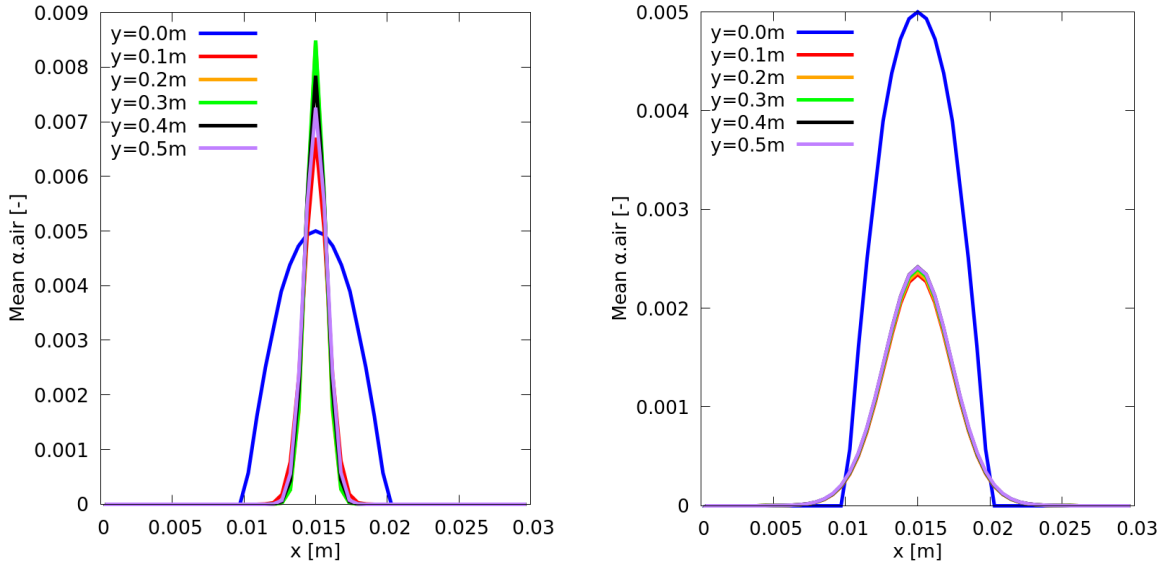

a) Standard Euler-Euler modelling b) Euler-Euler simulation based on particle-center-averaging

Figure 5: Lateral gas volume fraction distribution in turbulent flow case

When the grids are refined from 2 mm to 0.6 mm, the peak of the gas volume fraction increases and the lateral region covered by the gas decreases significantly (see Fig. 3 a)).

Axial development of gas volume fraction

In this section, the axial development of the distribution of the gas volume fraction in the two-dimensional test case is analyzed to show the improvement of the predictions obtained by the particle-center-averaged method. The mesh size for all the simulation cases in this section is 0.6 mm. It should be noted that for the inlet conditions as described above, the relative velocity between gas and liquid has a value of -0.02 $m{\cdot}s^{-1}$~$0.18 m{\cdot}s^{-1}$. However, the terminal velocity, which will be approached by the bubble as it rises is about 0.23 $m{\cdot}s^{-1}$ according to the correlation of Mendelson (Mendelson, 1967). Hence, the relative velocity will increase within a certain distance from the inlet.

Laminar flow case

In the simulations of the laminar flow case by the standard Euler-Euler modelling (see Fig. 4 a)), the gas moves to the channel center downstream of the inlet. A nonphysical peak of the gas volume fraction appears with an increasing distance. In addition, the lateral region covered by the gas becomes smaller than the bubble diameter and its extent decreases further downstream. This is nonphysical since the bubble size is expected to remain unchanged. As mentioned before, these phenomena are caused by the lift force being distributed to the bubble volume instead of acting on the bubble center.

In contrast, by using the particle-center-average based Euler-Euler modelling, the distribution of gas volume fraction remains almost unchanged after a short transient next to the inlet (see Fig. 4 b)). Further downstream, the lateral region covered by the gas has a size close to the bubble diameter. The increase of relative velocity right after the inlet causes the decrease of the peak of gas volume fraction. In conclusion, the predictions of the distributions of the gas volume fraction using the particle-center-averages are considered more reasonable.

Turbulent flow case

If the turbulent dispersion force is included, the nonphysical behaviours in the standard Euler-Euler modelling are weakened but remain visible in the results (see Fig. 5 a)). The lateral region covered by the gas downstream of the inlet is still smaller than the bubble diameter. Additionally, the peak of the gas volume fraction downstream is higher than that at the inlet. However, it should be lower than that at the inlet because of the increase of relative velocity with increasing distance from the inlet. In comparison, upon using simulation based on the particle-center-averages (see Fig. 5 b)), after a short distance downstream of the inlet, the distribution of the gas volume fraction remains almost unchanged and the size of the lateral region covered by the gas is close to the bubble diameter and remains constant. The simulation results of the gas volume fraction using the particle-center-averages are more physical because the lift force acts only on the bubble center.

In conclusion, the particle-center-averaging can help to avoid the overconcentration of gas around the location of the bubble center and provide a mesh independent solution.

COMPARISON OF SIMULATION RESULTS AND EXPERIMENTAL DATA IN PIPE FLOW

In order to evaluate the particle-center-averaged method in the Euler-Euler modelling, the simulation results of the standard Euler-Euler modelling and the Euler-Euler simulation based on the particle-center-averages are compared with measurement data from the MTLoop experiment (Lucas et al., 2005).

The test section in the MTLoop facility is a vertical pipe. Its inner diameter is 51.2 mm. The temperature of air and water in the experiment is 30℃ and the pressure is atmospheric pressure. The data used for comparison are measured at a distance of 3.03 m from the location of the gas injection. The ratio between the distance from the inlet and the pipe diameter (L/D) is about 59. Therefore, fully-developed flow is expected at the measurement location.

The inlet velocities and the volume fractions are uniform for disperse and continuous phases in the simulation. They are calculated from the superficial air and water velocities in the experiment. The parameters of the selected cases are listed in Table 2.

Table 2: Parameters of selected MTLoop cases

Test No.	J_{air} [$\mathrm{m \cdot s^{-1}}$]	J_{water} [$\mathrm{m \cdot s^{-1}}$]	d_B [mm]
017	0.0040	0.4050	4.865
019	0.0040	1.0170	4.697
042	0.0096	1.6110	4.151
043	0.0096	2.5540	2.918
047	0.0151	0.1020	7.442
048	0.0151	0.1610	6.486
064	0.0235	1.6110	4.661

The bubble diameters listed in this table are the Sauter mean diameters at the height of 3.03 m. In the simulation, the radial mesh size is 0.512 mm. It is uniform and finer than the bubble diameter.

First of all, the necessity of damping the lift force near wall in the simulations using the standard Euler-Euler modelling is illustrated. The radial distribution of the lift forces with and without near wall damping are shown in Fig. 6. As can be seen, without damping the lift force assumes extremely large values near the wall. This is due to the fine grid with a spacing smaller than the bubble size.

The effects of damping the lift force near wall on the distribution of the gas volume fraction in the cases simulated by the standard Euler-Euler modelling can be seen in Fig. 7. Without damping the lift, the peaks of the gas volume fraction in the simulation results can be much higher than the experimental data and locate directly on the wall. These peaks should locate at about one bubble radius away from the wall in the condition without

considering bubble deformations. The reason for this unphysical phenomenon is that the lift force is too high in near wall region. In comparison, the peak value and location simulated by damping the lift force have a better agreement with the experimental data. As a consequence, the wall-damping lift force is used in the following simulations.

The comparison of the radial distributions of the gas volume fraction to those simulated by the particle-center-averaged Euler-Euler modelling and the standard Euler-Euler modelling and the experimental data is shown in Fig. 8. The over-prediction of the peak of the gas volume fraction in the results calculated by the standard Euler-Euler modelling can be seen in these figures. The extent of the over-prediction is more severe for the cases with smaller bubble Sauter mean diameters.

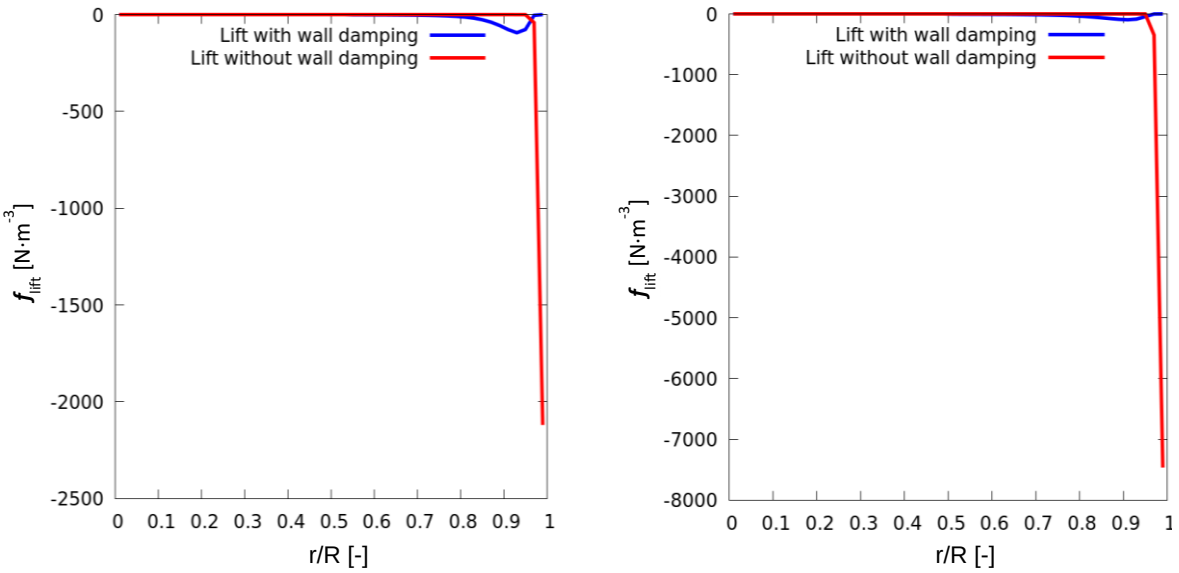

a) MTLoop 042 b) MTLoop 064

Figure 6: Radial distribution of lift force in cases simulated by standard Euler-Euler modelling

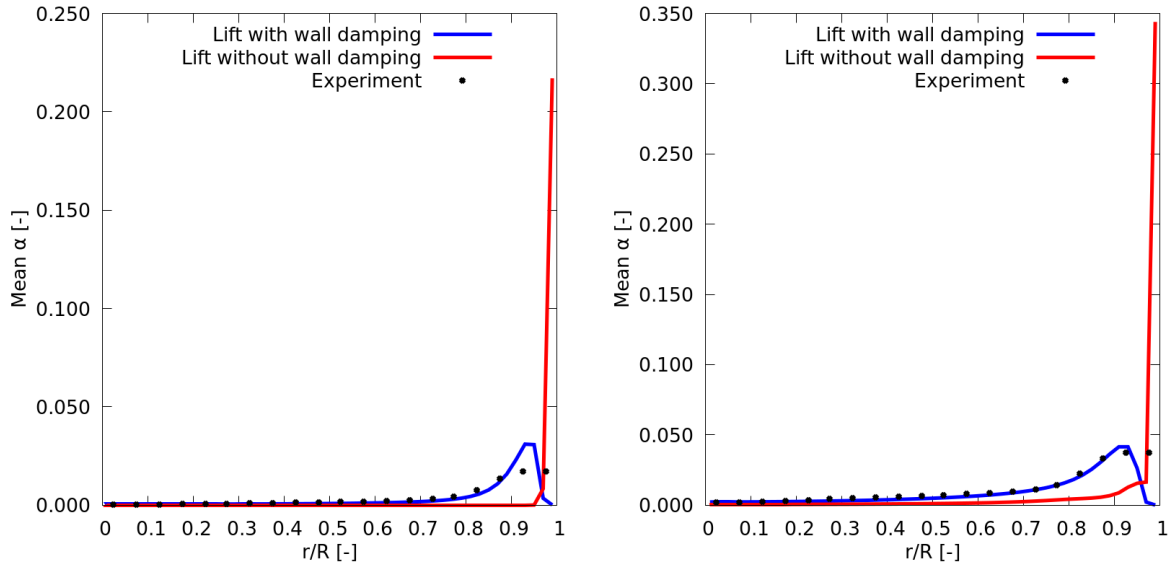

a) MTLoop 042 b) MTLoop 064

Figure 7: Radial distribution of gas volume fraction in cases simulated by standard Euler-Euler modelling

For case MTLoop 043, the peak value of gas volume fraction in the simulation result is about 10 times higher as in the experimental data. The over-prediction of the peak value for the gas volume fraction can be caused by the distributed lift force over the bubble volume in the standard Euler-Euler modelling. Furthermore, the reason of more significant over-prediction of the peak for smaller bubbles where the ratio of bubble diameter and mesh size is smaller can be that with the presently applied lift force correlation, the smaller bubble in these simulation cases experiences a higher lift force.

In comparison, the particle-center-averaged method displays its ability to avoid the over-prediction of the peak of the gas volume fraction in the near wall region. The peaks of the gas volume fraction simulated by the Euler-Euler based on the particle-center-averaged method fit the experimental data well in the majority of cases. The most notable deviation in these results is that the peak location is further away from the wall compared to the experimental data and the simulation results of the standard Euler-Euler modelling. This may result from using wall-lift and wall-contact forces at the same time could drive too much gas away from the wall.

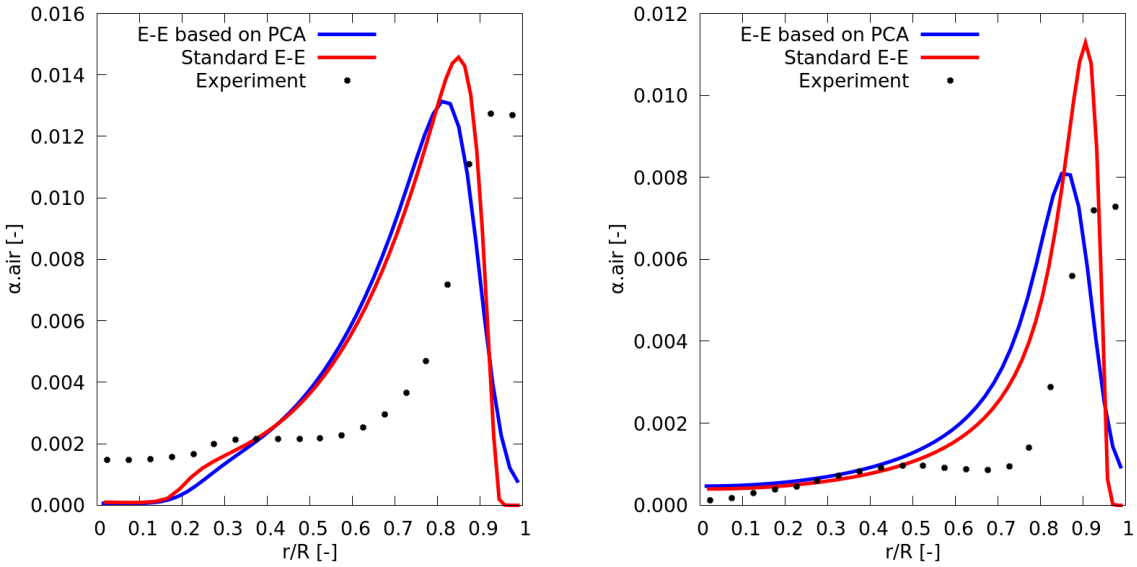

a) MTLoop 017

b) MTLoop 019

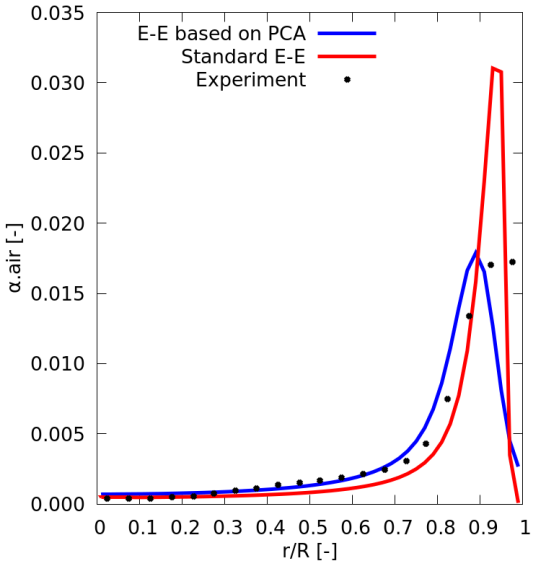

c) MTLoop 042

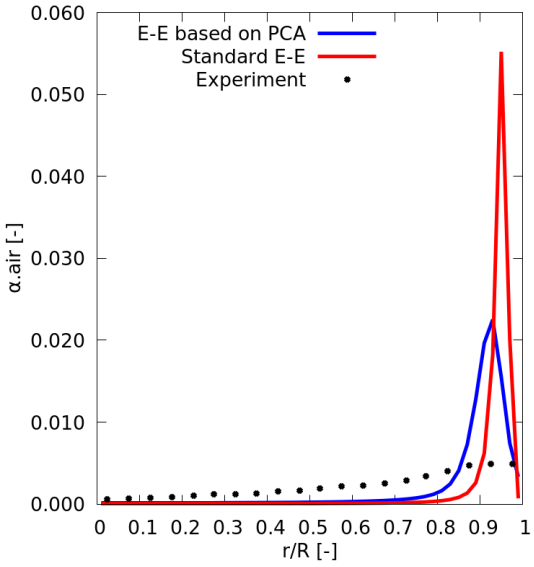

d) MTLoop 043

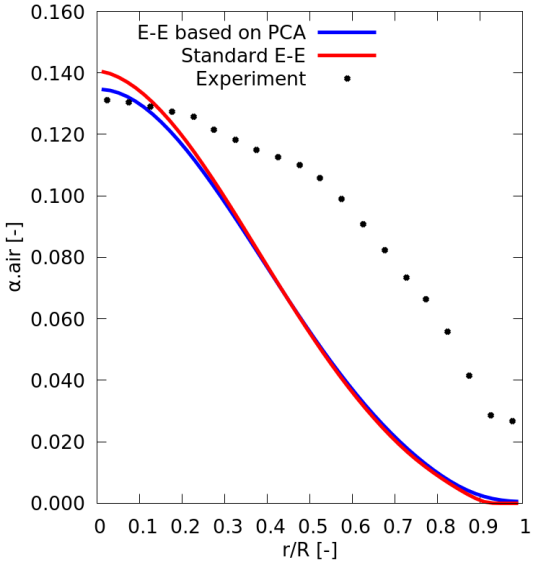

e) MTLoop 047

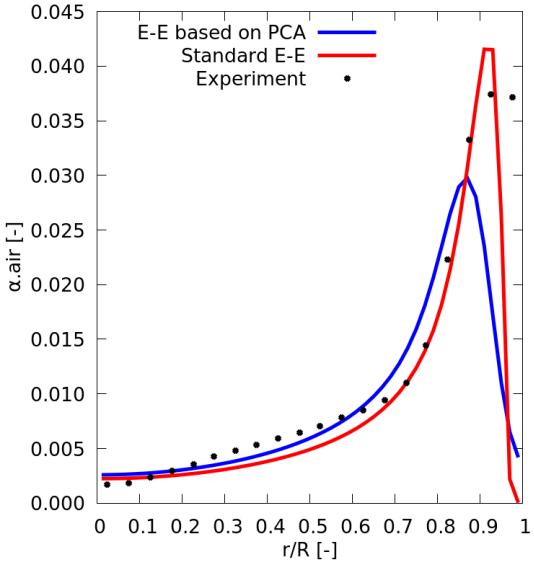

f) MTLoop 064

Figure 8: Radial distribution of gas volume fraction at 3.03 m downstream of the inlet with wall-damping lift force (E-E: Euler-Euler, PCA: particle-center-average)

CONCLUSION AND OUTLOOK

Inconsistencies exist in the standard Euler-Euler modelling based on the phase-averages since the forces of bubble are the function of gas volume fraction. When the bubble size exceeds that of the numerical mesh, the distributed lift force in bubble volume can lead to an over-prediction of the peak of the gas volume fraction. Refining the numerical mesh may lead to the increasing over-prediction of the peak value and mesh independent solution may not exist.

The diffusion-based particle-center-averaged method has been shown to remedy these inconsistencies. In this method, the forces act on the bubble center and the bubble dimension is considered in the process of using the diffusion-based method to transfer the number density of bubble canters into the gas volume fraction. A deformation force is employed to prevent the bubble centers to come arbitrarily close to the walls. As a result, the unphysical over-predictions of the peak value of the gas volume fraction near a wall or in the pipe center are alleviated or eliminated compared to the results of the standard Euler-Euler modelling. Numerically, the benefit of using this method is that the mesh-independent solutions exist.

In the Euler-Euler simulations based on the particle-center-averaged method, the forces acting on the continuous phase should still be distributed to the region covered by the bubble. Since this work is still in process, it has not been shown here. Furthermore, the future work should be focused on the research of near wall forces to avoid driving too much gas away from the wall.

REFERENCES

Biesheuvel, A. and W. Gorissen (1990), "Void fraction disturbances in a uniform bubbly fluid", *International Journal of Multiphase Flow*, **16**, 211-231.

Biesheuvel, A. and S. Spoelstra (1989), "The added mass coefficient of a dispersion of spherical gas bubbles in liquid", *International journal of multiphase flow*, **15**, 911-924.

Deen, N. G., M. van Sint Annaland, et al. (2004), "Multi-scale modeling of dispersed gas–liquid two-phase flow", *Chemical Engineering Science*, **59**, 1853-1861.

Drew, D. A. and S. L. Passman (1998). Theory of multicomponent fluids, Springer Science & Business Media.

Haberman, R. (2012). Applied partial differential equations with Fourier series and boundary value problems, Pearson Higher Ed.

Hu, G. and I. Celik (2008), "Eulerian–Lagrangian based large-eddy simulation of a partially aerated flat bubble column", *Chemical Engineering Science*, **63**, 253-271.

Khawaja, H. A., S. A. Scott, et al. (2012), "Quantitative analysis of accuracy of voidage computations in CFD-DEM simulations", *The Journal of Computational Multiphase Flows*, **4**, 183-192.

Kitagawa, A., Y. Murai, et al. (2001), "Two-way coupling of Eulerian–Lagrangian model for dispersed multiphase flows using filtering functions", *International journal of multiphase flow*, **27**, 2129-2153.

Lubchenko, N., B. Magolan, et al. (2018), "A more fundamental wall lubrication force from turbulent dispersion regularization for multiphase CFD applications", *International Journal of Multiphase Flow*, **98**, 36-44.

Lucas, D., M. Beyer, et al. (2010), "A new database on the evolution of air–water flows along a large vertical pipe", *International Journal of Thermal Sciences*, **49**, 664-674.

Lucas, D., E. Krepper, et al. (2005), "Development of co-current air–water flow in a vertical pipe", *International Journal of Multiphase Flow*, **31**, 1304-1328.

Lucas, D., E. Krepper, et al. (2007), "Use of models for lift, wall and turbulent dispersion forces acting on bubbles for poly-disperse flows", *Chemical Engineering Science*, **62**, 4146-4157.

Ma, T., C. Santarelli, et al. (2017), "Direct numerical simulation–based Reynolds-averaged closure for bubble-induced turbulence", *Physical Review Fluids*, **2**, 034301.

Mendelson, H. D. (1967), "The prediction of bubble terminal velocities from wave theory", *AIChE Journal*, **13**, 250-253.

Moraga, F., A. Larreteguy, et al. (2006), "A center-averaged two-fluid model for wall-bounded bubbly flows", *Computers Fluids*, **35**, 429-461.

Peng, Z., E. Doroodchi, et al. (2014), "Influence of void fraction calculation on fidelity of CFD‐DEM simulation of gas‐solid bubbling fluidized beds", *AIChE Journal*, **60**, 2000-2018.

Prosperetti, A. (1998), Ensemble averaging techniques for disperse flows, *Particulate Flows*, Springer, 99-136.

Rzehak, R., T. Ziegenhein, et al. (2017), "Unified modeling of bubbly flows in pipes, bubble columns, and airlift columns", *Chemical Engineering Science*, **157**, 147-158.

Sangani, A. S. and A. Didwania (1993), "Dispersed-phase stress tensor in flows of bubbly liquids at large Reynolds numbers", *Journal of Fluid Mechanics*, **248**, 27-54.

Sun, R. and H. Xiao (2015a), "Diffusion-based coarse graining in hybrid continuum–discrete solvers: Applications in CFD–DEM", *International Journal of Multiphase Flow*, **72**, 233-247.

Sun, R. and H. Xiao (2015b), "Diffusion-based coarse graining in hybrid continuum–discrete solvers: Theoretical formulation and a priori tests", *International Journal of Multiphase Flow*, **77**, 142-157.

Tomiyama, A., N. Shimada, et al. (2003), "Application of Number Density Transport Equation for the Recovery of Consistency in Multi-Field Model", *ASME/JSME 2003 4th Joint Fluids Summer Engineering Conference*, American Society of Mechanical Engineers.

Xiao, H. and J. Sun (2011), "Algorithms in a robust hybrid CFD-DEM solver for particle-laden flows", *Communications in Computational Physics*, **9**, 297-323.

Zhang, D. and A. Prosperetti (1994a), "Averaged equations for inviscid disperse two-phase flow", *Journal of Fluid Mechanics*, **267**, 185-219.

Zhang, D. and A. Prosperetti (1994b), "Ensemble phase‐averaged equations for bubbly flows", *Physics of Fluids*, **6**, 2956-2970.

Zhang, D. and A. Prosperetti (1995), "Energy and momentum equations for disperse two-phase flows and their closure for dilute suspensions", *J. Fluid Mech*.